Single Molecule Studies Enabled by Model-Based Controller Design

Shreyas Bhaban, *Student Member, IEEE*, Saurav Talukdar, *Student Member, IEEE*, Mingang Li, Thomas Hays, Peter Seiler, *Member, IEEE*, and Murti Salapaka, *Senior Member, IEEE*

***Abstract*—Optical tweezers have enabled important insights into intracellular transport through the investigation of motor proteins, with their ability to manipulate particles at the microscale, affording femto newton force resolution. Its use to realize a constant force clamp has enabled vital insights into the behavior of motor proteins under different load conditions. However, the varying nature of disturbances and the effect of thermal noise pose key challenges to force regulation. Furthermore, often the main aim of many studies is to determine the motion of the motor and the statistics related to the motion, which can be at odds with the force regulation objective. In this paper, we propose a mixed objective H_2/H_∞ optimization framework using a model-based design, that achieves the dual goals of force regulation and real-time motion estimation with quantifiable guarantees. Here, we minimize the H_∞ norm for the force regulation and error in step estimation while maintaining the H_2 norm of the noise on step estimate within user specified bounds. We demonstrate the efficacy of the framework through extensive simulations and an experimental implementation using an optical tweezer setup with live samples of the motor protein "kinesin", where regulation of forces below 1 piconewton with errors below 10% is obtained while simultaneously providing real-time estimates of motor motion.**

***Index Terms*—Acousto-optic deflector (AOD), intracellular transport, kinesin motility assay, mixed objective H_2/H_∞ optimization, molecular motor proteins, optical force clamp, optical trapping, system identification.**

Manuscript received October 3, 2017; revised March 2, 2018; accepted May 18, 2018. Date of publication July 2, 2018; date of current version August 14, 2018. Recommended by Technical Editor Y. K. Yong. This work was supported by the National Science Foundation (http://www.nsf.gov/) under Grant CNS 1544721. *(Shreyas Bhaban and Saurav Talukdar contributed equally to this work.) (Corresponding author: Murti Salapaka.)*

S. Bhaban and M. Salapaka are with the Department of Electrical Engineering, University of Minnesota, Minneapolis, MN 55455 USA (e-mail: bhaba001@umn.edu; murtis@umn.edu).

S. Talukdar is with the Department of Mechanical Engineering, University of Minnesota, Minneapolis, MN 55455 USA (e-mail: taluk005@umn.edu).

M. Li and T. Hays are with Department of Genetics Cell Biology and Development, University of Minnesota, Minneapolis, MN 55455 USA (e-mail: minga001@umn.edu; haysx001@umn.edu).

P. Seiler is with Department of Aerospace Engineering and Mechanics, University of Minnesota, Minneapolis, MN 55455 USA (e-mail: seile017@umn.edu).

Color versions of one or more of the figures in this paper are available online at http://ieeexplore.ieee.org.

Digital Object Identifier 10.1109/TMECH.2018.2852367

I. Introduction

TRANSPORT of important cargo inside the cells of eucaryotic species occurs through molecular motor proteins: kineisn, dynein, and myosin. These motor proteins enable directed transport of cargo by converting chemical energy to mechanical energy and are central to the regulatory mechanisms that maintain the internal organization of the cell [1], [2]. Structurally, the motor proteins are composed of a cargo binding tail domain, a stalk and two motor heads, where the motor heads bind to the microtubule filaments while transporting the cargo as shown in Fig. 1. The tail domain attaches to the cargo of interest, while the motor heads take discrete steps (or *walk*) over the pathways, composed of microtubules, inside the cell [3], thereby enabling directed transport of intracellular cargo. The typical motion of a single motor protein constitutes of series of discrete stepping events [4]. Motor proteins enable crucial intracellular functions, from producing muscle contraction and cellular tension to transport of subcellular organelles. Thus, proper functioning of molecular motors is indispensable in order to maintain a healthy cellular environment. Disruption of transport mechanisms due to impaired motor protein behavior is known to cause a host of maladies, including neurodegenerative diseases such as Huntington's, Parkinson's, and Alzheimer's [5], [6], high blood pressure, and muscular disorders such as heart disease.

Challenges in investigation of motor motion through direct observation (using, for example, confocal or transmission electron microscopy) stem from the extremely small dimensions and step sizes of the motor proteins. For example, kinesin is about 110 nm in length and takes 8-nm sized steps, while exerting forces in the range of pico newtons on the cargo. An efficient method of probing molecular motors is through the use of optical traps [9], [10], which use a laser beam focused through a high numerical aperture (NA) objective to trap micron-sized dielectric beads suspended in a suitable liquid medium, as shown in Fig. 2. When the beam is passed through a high NA objective, the interaction of the bead with the reflected and refracted rays of the laser, results in formation of a stable equilibrium point near the focus of the objective [11]. For small values of bead displacement, Δx, from the equilibrium point, the trap exerts a restoring force F_{trap} on the bead that is directed toward the trap location. F_{trap} varies linearly with the displacement following the relationship $F_{\text{trap}} = K_t \Delta x$, where K_t is the stiffness of the trap. The displacement of the bead can be measured up to

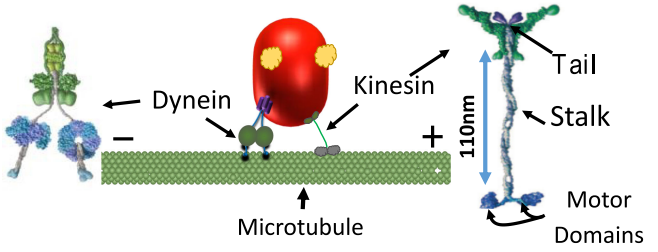

Fig. 1. Schematic showing intracellular cargo carried by motor proteins kinesin and dynein over a section of the microtubule inside the cell. Kinesin pulls the cargo toward the "plus" end of the microtubule while dynein primarily pulls the cargo toward the "minus" end of the microtubule.

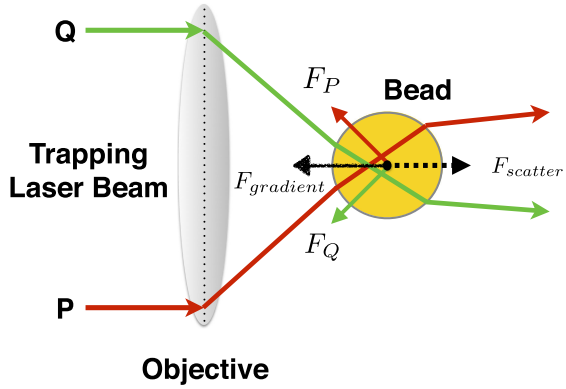

Fig. 2. Bead in an optical trap, as described in [7]. When the trapping laser beam is passed through a high numerical aperture objective, microscopic particles (such as the spherical bead) in the vicinity of the focus of the objective experience two kinds of forces (scattering and gradient forces) due to the transfer of momentum from the reflected and refracted rays of the laser onto the particle. F_P and F_Q are the reaction forces felt by the bead due to the momentum transfer from the rays P and Q, respectively. The destabilizing *scattering forces* F_{scatter} generated by the laser beam are balanced by the *gradient forces* F_{gradient} resulting from the Gaussian intensity profile of the laser, thereby creating a stable equilibrium point, i.e. an 'optical trap'.

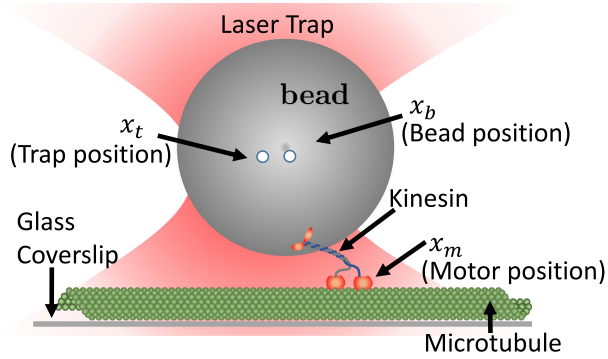

Fig. 3. Investigation of bead attached to motor protein "kinesin" using an optical trap. x_t, x_b, and x_m denote the trap location, bead position, and motor position, respectively.

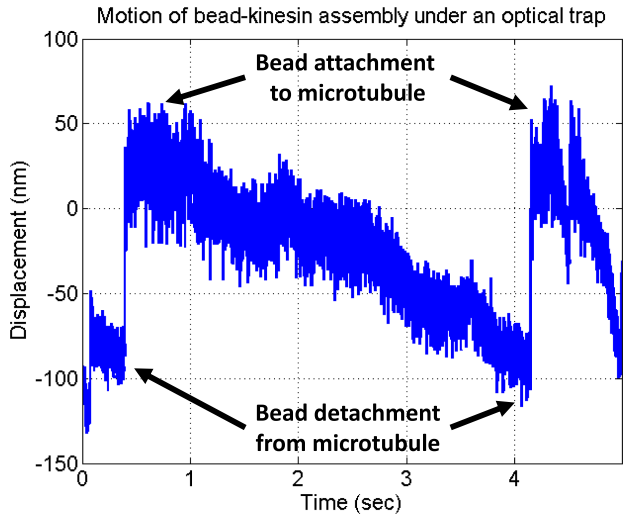

Fig. 4. Bead position data x_b gathered using position sensor (photodiode), with the bead in an optical trap while simultaneously traversing along the microtubule via the motor protein kinesin attached to it. When the optical trap is held stationary, it exerts more and more force on the bead as the bead is pulled further away from the trap focus. With increasing force on the bead, it is likely that the motors pulling the bead detach from the microtubule, at which point the bead is pulled back toward the focus of the trap due to the restoring force of the trap. This figure shows the sawtooth-like patterns [8] characteristic of the bead motion due to the attached molecular motors.

a limited range but with subnanometer resolution using photo diodes, whereas high bandwidth cameras yield larger range with resolution in micrometers [12], [13]. The position of the bead can be controlled by manipulating the position of the trapping laser, using actuators such as galvo mirrors (with bandwidth in Hz) and acousto-optic deflectors (AOD; with bandwidth in KHz). Optical traps have enabled force resolution on the order of femto-newtons and position resolution on the order of nanometers, proving successful in the study of a variety of nanoscale systems such as transport inside cells [9], [14], separation of microscopic objects [15], [16], etc.

To facilitate the investigation of motor proteins and detection of the stepping motion (denoted by x_m in Fig. 3) using optical traps, motor proteins are attached to spherical dielectric beads using appropriate biochemistry (see [17]). The beads act as cargo that can be trapped using an optical trapping setup. An *in-vitro* environment mimicking the habitat inside the cell is created in a glass chamber, where microtubule filaments are coated at the base of the glass chamber. Using the principles of optical trapping [7], [11], the cargo is trapped and brought close to the microtubules, to allow for the motor proteins connected to the cargo to attach to the microtubule as shown in Fig. 3. Once attached, the motor protein takes steps on the microtubule, while pulling the bead. An instance of the bead position measured by a photodiode sensor is shown in Fig. 4. The stepping data collected enables inference of important statistics of molecular motors such as motor detachment rates, stepping rates, and reattachment rates, which inform several widely used models of motor proteins. The models have enabled numerous important results on intracellular transport by single and multiple motor proteins [18]–[22].

Although measured bead position (such as that shown in Fig. 4) yields stepping statistics of the attached motor proteins, the motor linkage stiffens under increasing load [23], [24] exhibiting nonlinear force extension characteristics. Thus,

bead displacement data yields an inaccurate measure of the motor-protein motion, often necessitating corrections (about 15% for forces beyond 1 pN) to compensate for the effect [24]. Furthermore, for bead position measurements such as those shown in Fig. 4, the restoring force on the bead varies as it travels under the influence of the trap. Thus, the motor takes every step under changing load conditions. Transport properties of motor proteins are known to be altered when loading conditions change; thus, making it difficult to study the effect of load forces on motor protein behavior.

Studies of molecular motors under constant forces using optical tweezers are made possible through the use of *constant force clamps* ([24], [25]). They are designed to make the optically trapped bead follow the motor protein motion by regulating the separation between bead and trap position, $(x_b - x_t)$ to a desired value e_d allowing for the approximation of motor linkage as a Hookean spring. It is equivalent to maintaining load force on the bead equal to $F_d = K_t e_d$, thus allowing for constant force studies. Furthermore, it enables the measured bead position to correctly reflect the motor motion, from which the motor stepping statistics can be extracted using a variety of offline step detection techniques [26], [27] without the need for ad-hoc corrections [24]. Constant force clamps manipulate the position of the trap x_t using suitable actuators.

The major challenges in the force regulation objective are due to the high bandwidth disturbance caused by motor motion and the large variance of the thermal noise affecting the cargo. State-of-the-art force clamps [24], [25] yield low bandwidths and are effective for studying motors moving at slow speeds. As alluded to earlier, elucidating the true motion of the motor protein remains the main objective; however, the measured bead motion is corrupted by thermal noise effects and thus presently the measured position of the bead is processed via offline methods [26], [27] to estimate the motor motion. Furthermore, existing methods regulate the load force on the bead but fail to take into account the affect of motor motion on the force experienced by the molecular motor itself. Thus, for studies of motor-protein-based transport of cargo, a method that simultaneously provides, accurate loading of the motor protein while it is in motion, and a high bandwidth and high resolution real-time estimate of motor motion, will be a significant enabler. Existing state-of-the-art [24], [25] is unable to accommodate such a multiobjective design.

Our Contribution: In this paper, we employ the mixed objective H_2/H_∞ framework described in [28] to address the the desired diverse set of objectives. Using the framework, it is possible to have regulation of load force as well as estimation of stepping motion as design objectives. Through simulations, we demonstrate the ability to regulate forces below 1 pN with errors below 10% on cargoes moving up to speeds of 160 nm/s, which is close to the observed kinesin *in-vitro* speeds. Such a capacity will enable constant force studies where low errors in force regulation is of critical importance [20], [21]. Further simulations demonstrate the ability to regulate forces on motors moving as fast as 1000 nm/s with errors below 17%, resulting in significantly improved force clamp capabilities for probing motors with larger step sizes (hence higher speeds [29]) and motors moving at native speeds [30]. Moreover, we demonstrate real-time estimation of motor motion for motors traveling at speeds up to 160 nm/s with the root mean squared (rms) error in step estimation below 5%, while simultaneously maintaining sub piconewton forces with regulation error below 10% (as mentioned earlier).

We implement the design on a custom-designed optical tweezer setup and demonstrate the performance on live samples of motor-protein kinesin. Experimentally, we are able to regulate forces below 1 pN with errors below 10% on motors moving up to 200 nm/s using *in-vitro* motility assays. Without sacrificing force regulation, we demonstrate real-time stepping estimation of motor motion at 55 nm/s. This constitutes the first such demonstration, in both simulations and experiments, of maintaining load forces below 1 pN with errors less than 10%, while simultaneously estimating motor motion in real time. A preliminary simulation study of the force clamps using robust control framework has appeared in [31] and a preliminary experimental demonstration of the force clamp on a system mimicking the motor motion (without using motor proteins) has appeared in [32]. This paper builds upon [31], [32], while accommodating the additional objective of reducing the effect of motor motion on the force experienced by the molecular motor. Along with the added objective, the design in this paper is able to achieve a notable improvement in the bandwidth of regulation of force on the bead over that reported in [31], [32]. It further presents a detailed computational and experimental implementation of the constant force clamp on live motor protein (kinesin) samples. It thus provides first such demonstration of a model-based control design framework on live motor protein samples.

The paper is organized as follows. Section II presents the mathematical modeling and characterization of the system. Section III presents the controller design using the mixed objective H_2/H_∞ framework described in [28] for the optical tweezer system. Here, we present simulation results for force regulation and real-time stepping estimation of motor motion in the presence of thermal noise. Section IV presents experimental implementation of the framework and the results associated with testing the design on live kinesin motor proteins. It is followed by conclusion in section V.

II. Modeling and Characterization

A. Experimental Setup

The custom built optical tweezer forms the experimental setup for realizing optical traps (Fig. 5), where an Nd:YAG trapping laser (CrystaLaser Inc., $\lambda = 1064$ nm, 500 mW) is expanded using appropriate optics to fill the back aperture of high NA objective (Nikon 100x, 1.4 NA, oil immersion). The optical trap is formed at the focal point where spherical polystyrene beads are trapped. The trapping laser passes through two-axis AOD (IntraAction Corp., DTD–274HA6) that precisely steers the beam in x–y plane in response to appropriate commands. To detect the bead position, a second detection laser (Point Source Inc., iFLEX 2000, 50 mW, $\lambda = 830$ nm) is used to map the image of the bead onto a quadrant photodiode (Pacific Silicon Sensors, QP50–6SD2). A neutral density filter is added in the path

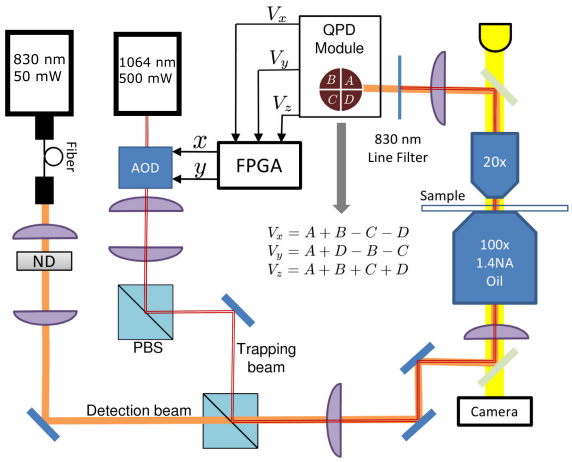

Fig. 5. Schematic for custom designed "optical tweezer' setup."

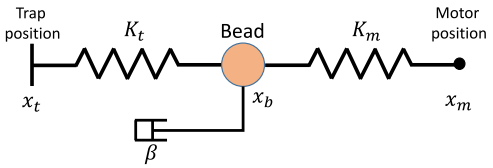

Fig. 6. Block diagram describing the open loop plant.

of the detection laser to reduce its intensity to ensure that it does not interfere with the trapping phenomenon. The photodiode enables the detection of the bead location by providing three signals V_x, V_y, and V_z, where V_x and V_y represent the photon distribution on the photodiode along x axis and y axis, respectively, while V_z corresponds to total light intensity. These signals are captured using FPGA-based data acquisition system (National Instruments, PCI 7833R) that generates appropriate commands for the AOD. The controller is implemented using Labview-based NI–FPGA.

B. System Model, Instrument Dynamics, and Actuator Characterization

Let the locations of the trap center, cargo, and motor head (on the microtubule) be denoted by x_t, x_b, and x_m, respectively. The bead in the optical trap is suspended in an aqueous medium with the coefficient of viscous damping β. For small magnitudes of displacement $x_b - x_t$ of the optically trapped cargo from the trap center, the force on the bead due to the optical trap is given by $K_t(x_b - x_t)$ [24]. Similarly, for small extensions $x_m - x_b$ of the motor stalk, the force on the cargo due to the motor protein is modeled as $K_m(x_m - x_b)$ [24], where K_m is the stiffness of the motor-stalk linkage. Under these conditions, the molecular motor carrying an optically trapped cargo (in this case, a spherical dielectric bead) can be modeled as a spring-mass-damper system with trap stiffness K_t, motor stiffness K_m, and the coefficient of viscous damping β, as shown in Fig. 6. The dynamics of the bead are observed to be highly overdamped [7], thus enabling the equation of motion of the bead in the presence of thermal noise η to be given by the following Langevin equation:

$$m\ddot{x_b} = -\beta\dot{x_b} + K_m(x_m - x_b) + K_t(x_t - x_b) + \eta. \quad (1)$$

The mass of the bead m is very small (of the order 10^{-17} kg), so (1) reduces to

$$\beta\dot{x_b} = K_m(x_m - x_b) + K_t(x_t - x_b) + \eta. \quad (2)$$

Applying Laplace transform to (2),

$$x_b(s) = G(s)(K_m x_m(s) + K_t x_t(s) + \eta(s)) \quad (3)$$

where $G(s) = \frac{1}{\beta s + K_t + K_m}$ and there is an abuse of notation with $x_m(s)$ used to represent the time and its Laplace transform as well.

In the absence of the motor (i.e., no motor attached to the bead) and thermal noise, the bead position in open loop follows the equation $x_b(s) = \frac{K_t}{\beta s + K_t} x_t(s)$. Let $G_p(s) = \frac{1}{\beta s + K_t}$. The trap position $x_t(s)$ can be manipulated using the command signal to the actuator $u(s)$ through the relation $x_t(s) = A(s)u(s)$, where the transfer function $A(s)$ models the dynamics of the actuator used to control the trap position. Thus, the position of the bead in open loop, in response to the command signal $u(s)$ is given by

$$x_b(s) = K_t G_p(s) A(s) u(s). \quad (4)$$

One of the primary reasons for the low bandwidth of the state-of-the-art force clamps is that they ignore dynamics of the actuator, i.e., the AOD [31], [32]. Given the inherent physics of the AOD, the dynamics need to be modeled accurately in order to design a force clamp that can accommodate slow as well as fast moving motors. In (4), the transfer function from the command input $u(s)$ to the measured bead position $x_b(s)$ is given by $G_h(s) = K_t G_p(s) A(s)$. We determine the expression for the actuator transfer function $A(s)$ from the experimentally identified expression for $G_h(s)$ using

$$A(s) = \frac{G_h(s)}{K_t G_p(s)} \quad (5)$$

where trap stiffness K_t and damping coefficient β are obtained by methods described in [24]. The transfer function $G_h(s)$ specific to the actuator and control hardware used to perform the experiments are identified by performing a chirp-wave-based system identification. A three-pole two-zero transfer function fit yields $G_h(s) = \frac{0.0396s^2 - 3160s + 1.101\times10^8}{1.7\times10^{-5}s^3 + 0.9967s^2 + 3.408\times10^4 s + 1.086\times10^8}$. Fig. 7 shows that the experimentally obtained step response shows a good match with the response predicted by the transfer function $G_h(s)$. Fig. 7 (blue curve) clearly demonstrates that the bead initially traverses in a direction opposite to the commanded direction, which is characteristic of the delays present in the AOD actuation system. The identified transfer function $G_h(s)$ (whose step response is shown in Fig. 7, red curve) contains a right half plane zero, that incorporates effects of delays, and by using (5) yields the actuator transfer function $A(s) = \frac{0.66s^2 - 5.267\times10^4 s + 1.835\times10^9}{s^2 + 5.51\times10^4 + 1.81\times10^9}$. The magnitude and frequency plots of $A(s)$ are shown in Fig. 8(a) and (b), respectively. Existing force clamps [24], [25] make the simplifying assumption of $A(s) = 1$ which is only appropriate for low frequencies and will lead to diminished performance at higher frequencies.

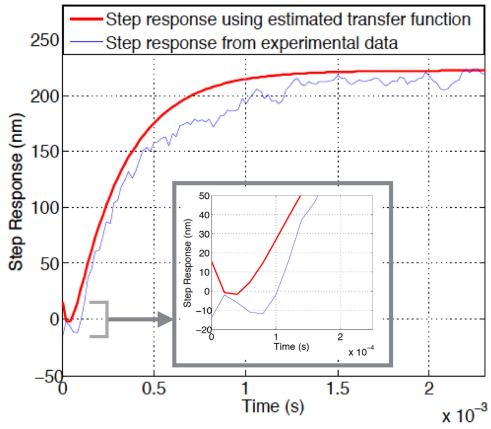

Fig. 7. Validation of the fitted transfer function $G_h(s)$ by comparing step responses. The experimentally obtained step response shows close agreement with that obtained using the fitted transfer function $G_h(s)$. Note the undershoot seen in both the experimental and simulation data (see inset) is characteristic of the delays present in the AOD system.

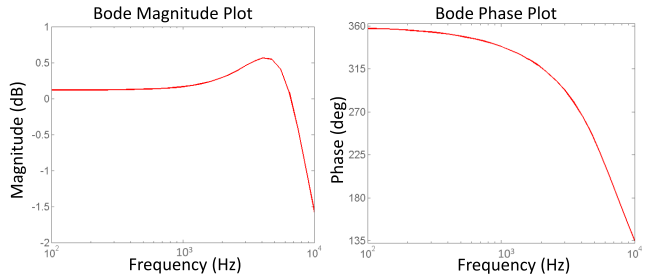

Fig. 8. Magnitude and phase plots for identified transfer function of the actuator, $A(s)$. Note that at high frequencies, magnitude reduces and phase delay increases, affecting the actuator response for input signals at high frequencies.

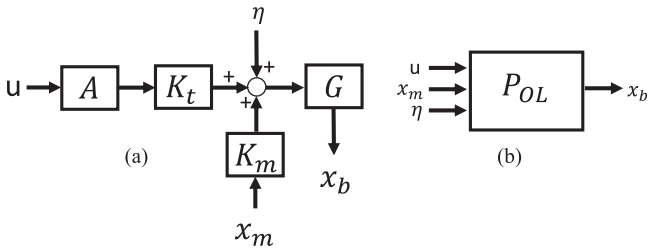

Fig. 9. Block diagram of the open loop plant P_{OL}. The inputs to the plant are u, x_m, and η, which denote the trap moment command, motor motion, and thermal noise, respectively, and are related by (3). The output x_b denotes the bead position as measured by the photo diode. As mentioned earlier, $G(s) = \frac{1}{\beta s + k_t + k_m}$ and $A(s)$ denotes the transfer function from trap command signal $u(s)$ to the trap position $x_t(s)$, thereby capturing the dynamics of the actuator (AOD).

Another way to identify the actuator transfer function is to model $G_h(s) = e^{-ts}\frac{C}{s+C}$, where t is the actuator delay and the constant $C = \frac{K_t}{\beta}$ incorporates the plant dynamics. A second-order Pade approximation of e^{-ts} yields a transfer function that matches the transfer function $A(s)$ obtained by the chirp-wave-based identification. The plant $G(s)$, actuator $A(s)$, trap stiffness K_t, and motor linkage stiffness K_m, together form the open loop plant P_{OL}, as shown in Fig. 9.

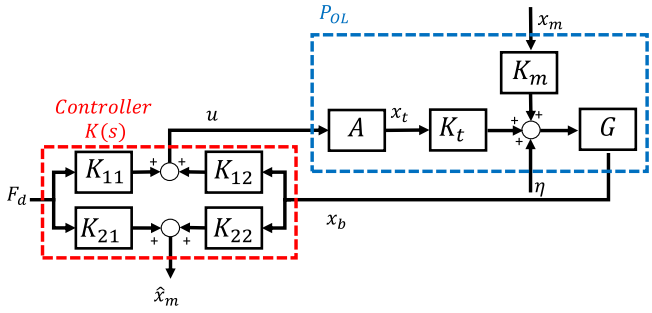

Fig. 10. Block diagram describing the closed-loop plant with open-loop plant P_{OL} and controller $K(s)$.

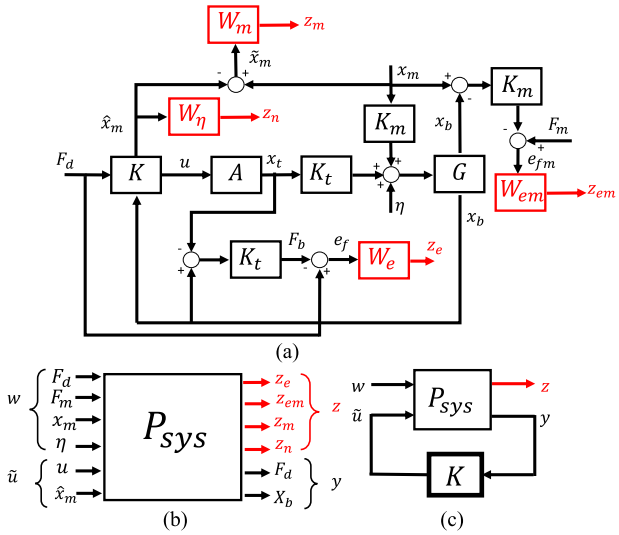

Fig. 11. (a) Block diagram of the plant with frequency dependent weights W_e, W_{em}, W_m, and W_η. (b) P_{sys} denotes the transfer function of the system with inputs $[w; \tilde{u}]$ and outputs $[z; y]$. (c) Closed-loop representation of the system with controller K.

In the next section, we present the mixed objective H_2/H_∞ framework utilized in order to design a controller that meets the multiple objectives of maintaining constant force on the bead and estimating the disturbance signal (motor stepping motion).

III. Controller Synthesis

The controller takes the desired force to be maintained, F_d, and the measured bead position, x_b, as its inputs and provides the command signal to the AOD u and the estimate $\hat{x}_m$ of the disturbance x_m as its outputs; thus, the controller $K(s)$ is a two-input two-output system as shown in Fig. 10. A block diagram describing the various components of the optical trapping system together with the feedback controller K is shown in Fig. 11(a). The performance objectives on the closed-loop system are as follows:

1) Good force regulation in the presence of set point changes and disturbances.
2) Accurate real-time estimation of motor motion.

The feedback diagram in Fig. 11 contains additional signals e_f and $\tilde{x}_m$ corresponding to the regulation error and estimation error, respectively. Input–output transfer functions appearing in

this loop are denoted via subscripts, e.g., $T_{e_f F_d}(s)$ denotes the transfer function from input F_d to output e_f. The desired performance objectives can be expressed in terms of specific transfer functions. The first objective translates to a requirement of small magnitudes for the transfer function $T_{e_f F_d}(s)$ and $T_{e_f X_m}(s)$.

Furthermore, the gain of the transfer function $T_{e_{fm} x_m}(s)$ is maintained to a small value, enabling the regulation of load force on the motor in the presence of motor motion. It also minimizes the effect of motor motion on extensions of the motor linkage, allowing for the motor linkage to be approximated as a Hookean spring. The second objective translates to a small gain for the transfer function $T_{\tilde{x}_m x_m}(s)$. The presence of the effect of thermal noise in the plant output x_b necessitates filtering out of the effect of the white noise from the disturbance estimate $\hat{x}_m$. This translates to reducing the effect of η (white noise) on $\hat{x}_m$, that is, minimize the gain of $T_{\hat{x}_m \eta}(s)$ across all frequencies. Note that the disturbance x_m and the noise η enter at the same location as shown in Fig. 11(a), so minimizing the H_2 norm of $T_{\hat{x}_m \eta}(s)$ is the same as minimizing the H_2 norm of $T_{\hat{x}_m x_m}(s)$. Another point to be noted is that, in the optical trapping system, the trap position x_t cannot be directly estimated for fast stepping motors (since $\frac{x_t(s)}{u(s)} = A(s) \neq 1$ at high frequencies); hence, it is not possible to design an effective feedback strategy that uses regulation error $e_f = F_d - k_t(x_b - x_t)$ as an input to the controller. The proposed framework enables desired objectives to be obtained without resorting to the regulation error e_f.

A. Design Objectives

The multiobjective output feedback control paradigm described out in [28] provides an effective controller synthesis approach to meet the desired objectives. The list below enumerates the desired performance requirements:

1) Minimize $\|[T_{e_f F_d}\ T_{e_f x_m}]\|_{H_\infty}$.
2) Minimize $\|[T_{e_{fm} x_m}]\|_{H_\infty}$.
3) Minimize $\|T_{\tilde{x}_m x_m}\|_{H_\infty}$.
4) Minimize $\|T_{\hat{x}_m x_m}\|_{H_2}$.

We incorporate a constraint on the H_2 norm $\|T_{\hat{x}_m x_m}\|_{H_2}$ as $\|T_{\hat{x}_m \eta}\|_{H_2}^2 < \nu$ in the optimization problem, where ν is specified by the user. Frequency-dependent weights $W_e(s)$, $W_{em}(s)$, $W_m(s)$, and $W_\eta(s)$ are introduced to penalize the signals e_f, e_{fm}, $\tilde{x}_m$, and $\hat{x}_m$, respectively, as shown in Fig. 11(a) and ensure feasibility of the optimization problem. Note that, $W_m(s)$ and $W_\eta(s)$ should emphasize nonoverlapping frequency regions, since the signals x_m and η enter the plant at the same location. We define the vector $z := [z_e, z_{em}, z_m, z_\eta]^T$ as the generalized output vector, $w := [F_d, F_m, x_m, \eta]^T$ as the vector of generalized input, $y := [F_d, x_b]^T$ as the input to the controller, and $\tilde{u} := [u, \hat{x}_m]^T$ as the output of the controller K. P_{sys} is the open-loop plant including the weights, as shown in Fig. 11(b) and is given as equation as shown bottom of this page.

The associated optimization problem to synthesize a controller $K(s)$ is given below:

$$\begin{aligned} &\min_{K(s),\gamma}\ \gamma \\ &\text{such that, } \|[T_{z_e f_d}\ T_{z_e x_m}]\|_{H_\infty} < \gamma \\ &\qquad \|[T_{z_{em} x_m}]\|_{H_\infty} < \gamma \\ &\qquad \|T_{z_m x_m}\|_{H_\infty} < \gamma \\ &\qquad \|T_{z_\eta \eta}\|_{H_2}^2 < \nu. \end{aligned} \tag{6}$$

Here,

$$\begin{aligned} T_{z_e f_d} &= W_e(s)(1 - GK_t^2 K_{11}(s)A(s)H(s) \\ &\quad + A(s)K_t K_{11}(s)H(s)) \\ T_{z_e x_m} &= W_e(s)K_t G(s)K_m((A(s)K_{12}(s) - 1)H(s)) \\ T_{z_{em} x_m} &= W_{em}(s)K_m G(s)K_t A(s)K_{12}(s)H(s) \\ T_{z_m x_m} &= W_m(s)(1 - G(s)K_m K_{22}(s))H(s) \\ T_{z_\eta \eta} &= W_\eta G(s)K_{22}(s)H(s) \end{aligned}$$

where $H(s) = \frac{1}{1 - K_t G(s)A(s)K_{12}(s)}$.

The above optimization problem is a convex optimization problem as shown in [28], the optimal solution to which is obtained by solving the corresponding Linear Matrix Inequalities (or LMI's). The solution scheme in [28] utilizes a common Lyapunov function for all the objectives, thereby bringing some amount of conservatism in the design process. However, the obtained controller is guaranteed to be stabilizing and also is of the same order as the plant, making it suitable for real-time implementation. The associated closed-loop system is shown in Fig. 11(c).

The weight $W_e(s)$ is chosen [Fig. 12(a)] to penalize the regulation error e_f, with gains below -16 dB for disturbances upto 700 Hz, corresponding to average motor velocity of motors of 5600 nm/s. It ensures small values of regulation errors at steady state as well as the frequencies of interest, corresponding to the observed native speeds of molecular motors [30]. $W_{\text{em}}(s)$ is chosen [Fig. 12(b)] to minimize the effect of motor disturbances on error e_{fm}, by maintaining the gain below -5 dB for disturbances upto 100 Hz corresponding to an average velocity of 800 nm/s, consistent with unloaded speeds of motor protein

$$P_{\text{sys}} = \begin{bmatrix} W_e & 0 & -W_e K_t K_m G & -W_e K_t G & W_e K_t A(1 - K_t G) & 0 \\ 0 & W_{em} & -W_{em} K_m (1 - K_m G) & W_{em} K_m G & W_{em} K_m G K_t A & 0 \\ 0 & 0 & W_m & 0 & 0 & -W_m \\ 0 & 0 & 0 & 0 & 0 & W_\eta \\ 1 & 0 & 0 & 0 & 0 & 0 \\ 0 & 0 & GK_m & G & GK_t A & 0 \end{bmatrix}$$

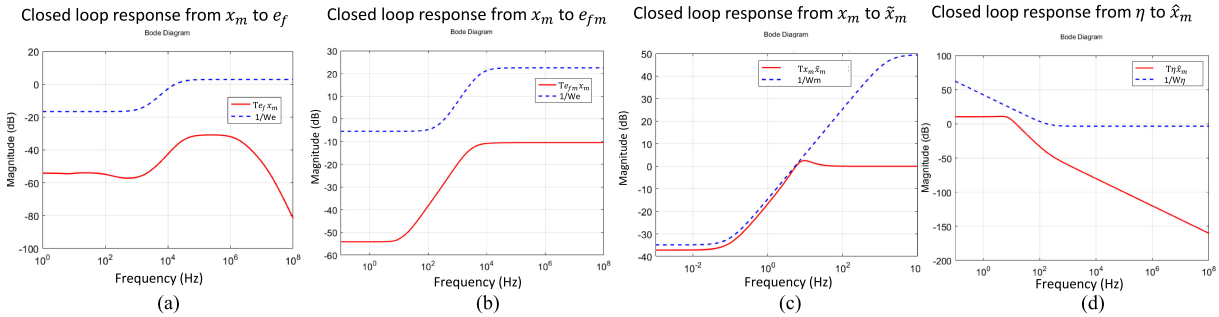

Fig. 12. Frequency response of (a) $T_{e_f x_m}(s)$ and $W_e^{-1}(s)$, (b) $T_{e_{fm} x_m}(s)$ and $W_{em}^{-1}(s)$, (c) $T_{\tilde{x}_m x_m}(s)$ and $W_m^{-1}(s)$, (d) $T_{\hat{x}_m x_m}(s)$ and $W_\eta^{-1}(s)$ using mixed objective H_2/H_∞ method. All three closed-loop transfer functions meet the desired frequency dependent performance for the chosen weights $W_e = \frac{0.5s+6000}{s+60}$, $W_{em} = \frac{0.075s+2700}{s+1440}$, $W_m = \frac{0.01s+100}{3s+1.8}$, and $W_n = \frac{1.194\times10^{-3}s}{7.958\times10^{-4}s+1}$.

kinesin [19], [20]. $W_m(s)$ is chosen [Fig. 12(c)] to minimize the effect of disturbances on estimation of motor motion, for motor speeds upto 160 nm/s, consistent with observed *in-vitro* speeds using the motility protocol designed in [17] (further details are provided in next section). $W_\eta(s)$ is chosen [Fig. 12(d)] to penalize the higher frequencies (>20 Hz) so that the estimate $\hat{x}_m$ is devoid of high frequency noise. $W_\eta(s)$ is also chosen such that it avoids an overlap of frequencies with the chosen weight $W_m(s)$, while also ensuring the feasibility of the optimization problem. The 2×2 controller

$$K(s) = \begin{bmatrix} K_{11}(s) & K_{12}(s) \\ K_{21}(s) & K_{22}(s) \end{bmatrix}$$

(shown in the closed-loop diagram in Fig. 10) is determined using the given frequency dependent weights and ν (=2.23) by solving the corresponding LMI's shown in [28]. The CVX solver [33] is utilized to solve for the corresponding LMI's (see [28] for more details on solving for LMI's) and returns a stabilizing controller $K(s)$ for the chosen weights and value of ν. The resulting optimal value of γ is obtained to be 2.63.

Note that $K_{21}(s)$ corresponds to the closed-loop transfer function from F_d to $\hat{x}_m$. It is evident that the transfer functions $\|[T_{z_e f_d} \;\; T_{z_e x_m}]\|_{H_\infty}$, $\|[T_{z_{em} x_m}]\|_{H_\infty}$, $\|T_{z_m x_m}\|_{H_\infty}$, and $\|T_{z_\eta \eta}\|_{H_2}^2$ in (6) do not depend on the the controller transfer function $K_{21}(s)$, implying that the estimate $\hat{x}_m$ does not depend on the reference signal F_d. Thus, setting $K_{21}(s) = 0$ in the optimal controller obtained by solving the set of LMIs and utilizing controller

$$\bar{K}(s) = \begin{bmatrix} K_{11}(s) & K_{12}(s) \\ 0 & K_{22}(s) \end{bmatrix}$$

does not alter the closed loop performances of the desired channels, as defined in (6). This simplifies the motor motion estimate $\hat{x}_m(s)$ to be $K_{22}(s)X_b$. $\bar{K}(s)$ is a 6th order controller with frequency response shown in Fig. 13. The frequency response of the inverse of the weights $W_e(s), W_{em}(s), W_m(s), W_\eta(s)$ and the corresponding closed loop transfer functions with the optimal controller in loop are shown in Figure 13. It is clear from the figure that the closed loop transfer functions meet the desired frequency dependent performance specifications.

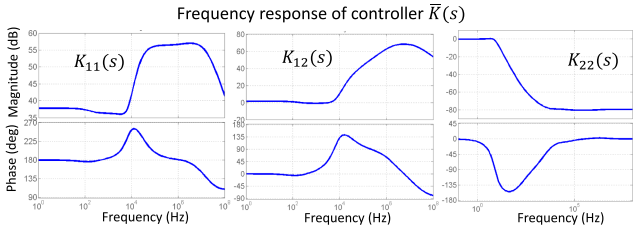

Fig. 13. Frequency responses of the controller $\bar{K}(s)$.

TABLE I
REGULATION AND ESTIMATION ERROR FOR VARIOUS MOTOR STEPPING FREQUENCIES

Step Rate (steps/s)	Motor Speed (nm/s)	$r(\%)$	$r_{rms}(\%)$	e_{rms}(nm)
5	40	4.85	6.1	5.21
10	80	7.42	8.29	4.83
15	120	8.06	8.87	4.78
20	160	8.40	9.18	4.88

B. Simulation Results

The performance comparison metric for regulation is the percentage regulation error, $r := \frac{\sigma(F_d - k_t(x_b - x_t))}{F_d} \times 100\%$ where $\sigma(.)$ denotes standard deviation; and percentage rms error, $r_{rms} := \frac{e_{\text{rms}}}{F_d} \times 100\%$ where e_{rms} is the rms value of the error $e = F_d - F_b$. The performance metric for estimation error, $e_{\text{rms}} := \sqrt{\langle \tilde{x}_m^2 \rangle}$, where $\langle . \rangle$ denotes the expectation operator. Table I lists the regulation and estimation error performance of the synthesized controller for $F_d = 0.95$ pN and x_m being a simulated staircase signal of 8 nm steps with frequencies of 5, 10, 15, 20 steps/s corresponding to average motor speeds of 40, 80, 120, 160 nm/s. It is seen that regulation error is less than 10% and the rms estimation error is less than 6 nm for *in vitro* motor stepping frequencies upto 160 nm/s. Fig. 14(a) shows an example of the estimate $\hat{x}_m$ of x_m using the noisy bead position x_b when the frequency of the steps is 5 Hz and Figure 14(b) shows the error in force regulation.

Thus, the synthesized controller achieves the desired objectives of force regulation and real-time motor motion estimation in simulations. In the next section, we demonstrate the experimental performance of the controller using live samples of the motor protein kinesin-I.

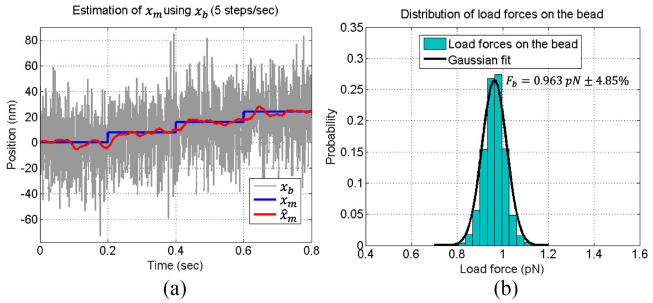

Fig. 14. (a) Realization of $\hat{x}_m$ computed using x_b when simulated x_m is a staircase signal with stepping frequency 5 Hz and (b) the distribution of the associated regulation error. The force on the bead is $F_b = 0.963\,pn \pm 4.85\%$ (1 s.d) with 6.1% rms error.

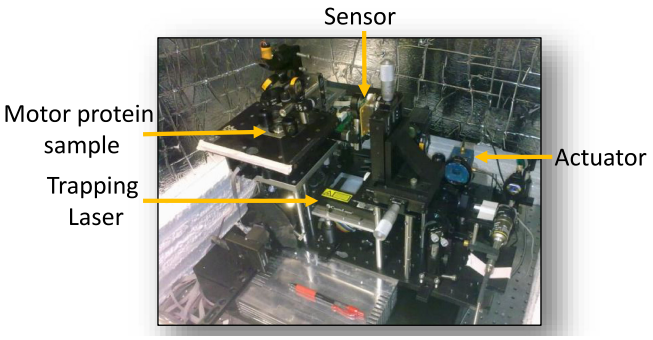

Fig. 15. Experimental setup for "Optical Tweezer." The pen has been placed to give an idea of the scale of the system.

IV. Experiments With Live Motor Proteins

In this section, we present an experimental implementation of the mixed objective $H_2 - H_\infty$ optical force clamp (designed in the previous section) on our optical tweezer setup (Fig. 15). The controller is implemented using an National Instruments $PCI7833R$ FPGA. The command signal u to the actuator, which regulates the load force on the bead at the reference value F_d is given by $K_{11}F_d + K_{12}x_b$, where x_b is the measured bead position. The estimated motor motion is obtained by $\hat{x}_m = K_{22}X_b$. The transfer functions K_{11}, K_{12}, and K_{22} are obtained in the continuous form and have to be discretized in order to be implemented using FPGA hardware. We utilize the bilinear transformation by substituting $s = \frac{2}{T}\frac{z-1}{z+1}$ to obtain the equivalent discrete-time transfer functions K_{11}, K_{12}, and K_{22}, where T is the sampling period of the system (50 KHz in this paper). Furthermore, we develop and implement a bead motility assay where carboxylated beads 1 μm in diameter are attached to kinesin-I motor protein using appropriate biochemistry. We then test the performance of the mixed objective clamp on the beads carried by live kinesin-I motors and compare it with the performance of existing state-of-the-art force clamps.

A. Procedure and Demonstration

To investigate motor protein motion using an optical force clamp, the optical tweezer is utilized to trap a polystyrene bead, with the bead being attached to kinesin-I motors using the protocol described in [17]. For the experiment, the trapped bead is brought close to the base of the glass slide where microtubule filaments have been previously coated (see [17] for details) and held stationary at a distance of ≈ 100 nm above it. As the kinesin protein attaches to the microtubule and gradually begins traversing, a unidirectional motion of the bead toward the positively charged end of the microtubule (similar to Fig. 4) is recorded using the photodiode sensor. The optical force clamp is designed to maintain a constant force of F_d on the bead, which is equivalent to maintaining a constant distance of $d = \frac{F_d}{K_t} = x_b - x_t$ between the locations of the bead and the trap. The clamp is designed to trigger only after the bead has moved more than a distance of d away from the trap focus, that is, after $x_b - x_t \geq d$. When $x_b - x_t < d$, the force clamp is not triggered and the trap position does not change in response to changes in the bead position. An instance of the force clamp in action for $d = 100$ nm is demonstrated in Fig. 16 (a), where zones 1, 2, and 3 denote the different stages of bead motion under the optical force clamp. A representation of the bead-motor assembly corresponding to each of the zones is shown in Fig. 16(b). In zone (1), the bead is trapped and being brought close to the microtubule, awaiting attachment of the motor. No directed motion of the bead is recorded. In zone (2), the motor attaches to the microtubule and pulls the bead, yet the force clamp is not triggered since $x_b - x_t < d$. In zone (3), $x_b - x_t \geq d$ and the force clamp is activated, which is seen in the corresponding section in the Fig. 16(a), where the trap position (red trace) follows the bead position (blue trace) and maintains the distance $x_b - x_t$ close to $d = 100$ nm. For the trap stiffness $K_t = 0.0095$ pN/nm, $d = 100$ nm translates to a desired force of $F_d = 0.950$ pN on the bead.

B. Results

The mixed objective $H_2 - H_\infty$ force clamp was tested on beads with average velocities ranging from about 59 nm/s to 193 nm/s (see Table II for details). The mixed objective force clamp demonstrated significantly improved regulation performance, with the error in force resolution ranging from 4.67% to 7.97% while having rms error below 10%. An instance of the force clamp operating on a bead travelling at 107 nm/s is shown in Fig. 17(a), where an error in force regulation of 6.075% is obtained [as shown in Fig. 17(b)]. We compared the performance of the existing state-of-the-art [24] under similar conditions of load force and velocities, where higher errors in force regulation were seen (as shown in Table III). An instance of the traditional force clamp operating on a bead travelling at 149 nm/s is shown in Fig. 18(a), where an error of 17.68% is obtained [Fig. 18(b)]. It is evident that the mixed objective approach provides an advantage over the existing approaches and is capable of regulating subpiconewton forces with errors below 10%.

We further utilized the mixed objective force clamp to provide with a real-time estimate $\hat{x}_m$ of the motor motion x_m. The estimate of the motor motion for an average velocity of 55 nm/s ($\approx$ stepping frequency of 7 steps/s) is shown by red curve in Fig. 19. Since the actual stepping signal is not known, an estimate obtained using state-of-the-art offline step estimation algorithm [27] (blue curve) is shown for comparison. It is

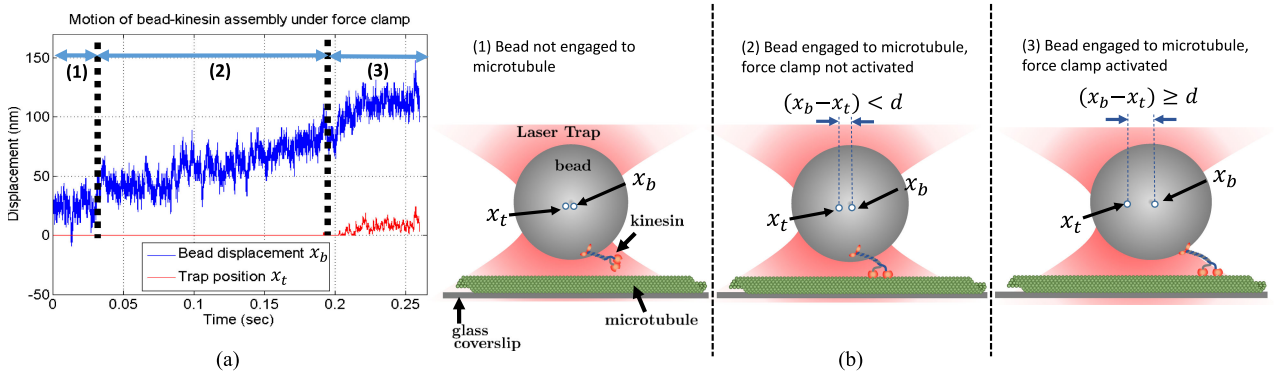

Fig. 16. (a) Sample trace of bead (x_b) and trap position (x_t) showing optical force clamp in action, divided into three zones. (b) Diagrammatic representation of the behavior of bead-kinesin ensemble in each of the three zones. In zone (1), the bead attached to kinesin is brought close to the glass surface and awaits the attachment of the kinesin to the microtubule filaments coated onto it. No motion of the bead is recorded as the kinesin does not attach to the microtubule. Once the attachment occurs as shown in zone (2), the motor pulls the bead and traverses along the microtubule in a directed manner. However, since the displacement of the bead position from the trap position is less than $d = 100$ nm, the force clamp is not triggered and the trap position x_t remains unchanged. Once $x_b - x_t > 100$ nm as seen in zone (3), the force clamp is triggered and the trap position follows the bead position while maintaining $x_b - x_t$ close to 100 nm.

TABLE II
$H_2 - H_\infty$ FORCE CLAMP REGULATION PERFORMANCE

Motor Speed in (nm/s)	r (%)	r_{rms} (%)
59.17	4.67	5.16
68.11	5.069	5.53
93.2	7.07	7.4
107.53	6.075	6.46
152.01	5.073	5.55
193.3	7.97	8.27

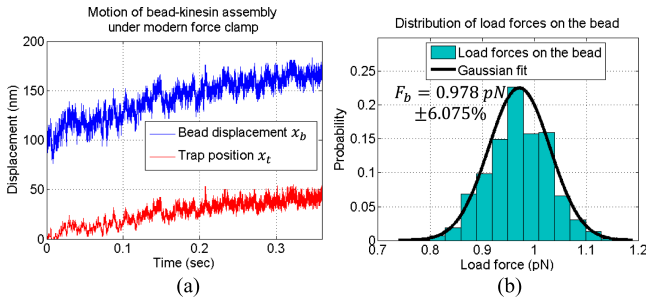

Fig. 17. (a) Sample trace of bead and trap position showing the modern H_2/H_∞ force clamp in action. (b) Distribution of the error in force regulation (6.46% rms error).

TABLE III
PERFORMANCE USING TRADITIONAL FORCE CLAMP [24]

Motor Speed in (nm/s)	r (%)	r_{rms} (%)
45.86	17.806	17.96
149.64	17.68	17.83

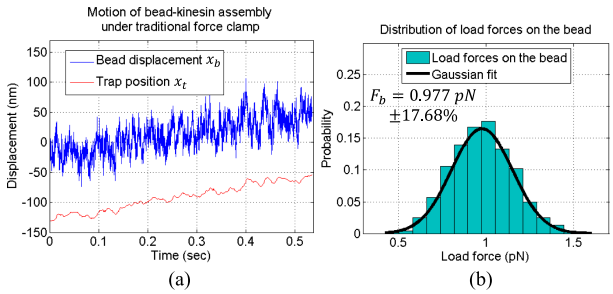

Fig. 18. (a) Sample trace of bead and trap position showing the traditional force clamp [24] in action (b) Distribution of the error in force regulation (17.83% rms error).

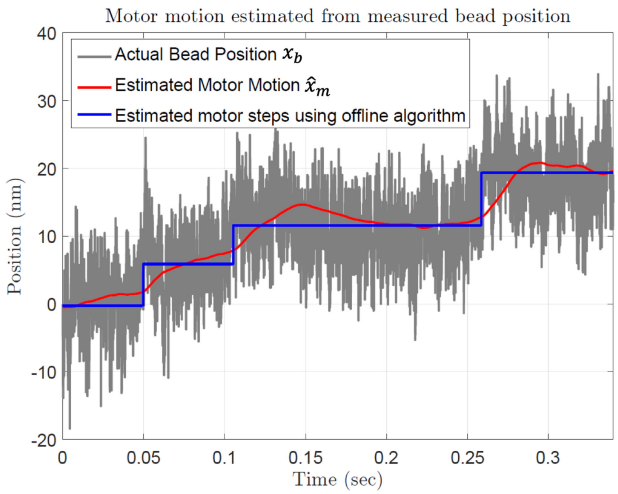

Fig. 19. Real-time estimation of stepping motion, with average bead velocity of 55 nm/s.

seen that the high frequency noise is filtered out, providing an estimate $\hat{x}_m$ comparable with state-of-the-art offline step estimation techniques.

Moreover, the estimated signal $\hat{x}_m$ can provide starting points or edges that can be used by machine learning or dynamic programming based algorithms to generate statistics in real time or with an acceptable amount of delay. Thus, the force clamp presented in this paper facilitates investigation and real-time estimation of motor motion under sub pN load forces, which to the best of our knowledge has not been reported in the existing studies.

V. Conclusion

This paper presents a detailed design for an optical force clamp using a mixed objective H_2/H_∞ framework, along with verifications using simulations as well as experiments using live motor proteins; with extensive applications to investigation of bio-molecules and processive motor proteins. The model-based approach using a systematic design methodology results in notable improvement in force regulation and bandwidth of operation over existing designs [24], [25]. A crucial enabler of the design is a precise understanding and modeling of hitherto un-modeled dynamics in the existing instruments using right half plane zeros; identified by a data-driven system identification approach. We verify the design through extensive numerical simulations, providing improved force regulation with guaranteed performances based on user-defined weight functions. The improved design can enable bio-molecular studies with higher resolution through the ability to investigate systems at finer intervals of forces. It will allow researchers to discover events that were not possible due to limitations of current designs, leading to possible refinement of bio-molecular models. The design allows for examining motor proteins at higher velocities close to their native speeds [30] and proteins with larger step sizes [29] with satisfactory force regulation. The design using modern control framework adds to the robustness of the system to parametric uncertainties. We further implemented the design on an optical tweezer setup and tested its efficacy using live samples of the motor protein "kinesin," demonstrating the ability to regulate subpico newton forces with errors below 10%; individual attempts are also shown to have errors below 5%.

The paper also proposes a scheme for real-time stepping estimation of molecular motors, which to the best of our knowledge is absent from current literature. By virtue of the mixed objective H_2/H_∞ design, we are able to reduce the effects of thermal noise on stepping estimate without compromising on the force regulation. We demonstrate the efficacy of the method using simulations as well as experiments involving live "kinesin" samples. Unlike some methods that reduce the effects thermal noise on stepping signal through stiffening the system [24], [34], our method preserves the dynamics of the system and thus avoids impacting the system being examined. The real-time step estimation methodology can prove to be of importance to experimental bio-physicists, equipping them with the ability to detect and identify motor protein motility in real time. To the best of the author's knowledge, our method is the first of its kind that demonstrates the force regulation with errors as low as 4.67% on samples of live motor protein kinesin, while simultaneously providing real-time estimates of the motor stepping motion. Note that the step estimation bandwidth for our method is limited to slow moving motors due to the tradeoff in the H_2/H_∞ cost over the identical channel. It is useful for motor proteins operating in the high load force and low ATP regimes [24], [35]. Future work entails exploiting the knowledge of the noise properties and designing the corresponding weight function (W_η in this paper) more efficiently. Nevertheless, our proposed scheme enables improved investigative abilities in molecular biology using system theory tools and provides improvement in force clamping abilities over current methods, with the added contribution of estimation of motor motion in real time. As future work, observer based ideas for fast detection of events in motor protein data will be targeted (see [36] and [37]). While the current work primarily uses time-domain objectives indirectly via frequency domain measures, we also plan to evaluate the effectiveness of the frameworks (see [38] and [39]) of directly posing time-domain objectives with time domain measures.

Acknowledgment

The authors would like to thank Subhrajit Roychowdhury, GE Global Research, for help with the optical trapping experiments and Tanuj Agrawal, Cymer for sharing his insights on optical tweezers. The discussions with Biswaranjan Mohanty and Sivaraman Rajaganapathy from the University of Minnesota have been insightful.

References

[1] E. L. Holzbaur and Y. E. Goldman, "Coordination of molecular motors: From in vitro assays to intracellular dynamics," *Current Opinion Cell Biol.*, vol. 22, no. 1, pp. 4–13, 2010.

[2] J. P. Caviston and E. L. Holzbaur, "Microtubule motors at the intersection of trafficking and transport," *Trends Cell Biol.*, vol. 16, no. 10, pp. 530–537, 2006.

[3] K. Svoboda, C. F. Schmidt, B. J. Schnapp, and S. M. Block, "Direct observation of kinesin stepping by optical trapping interferometry," *Nature*, vol. 365, no. 6448, pp. 721–727, 1993.

[4] C. L. Asbury, A. N. Fehr, and S. M. Block, "Kinesin moves by an asymmetric hand-over-hand mechanism," *Science*, vol. 302, no. 5653, pp. 2130–2134, 2003.

[5] M. A. Welte, S. P. Gross, M. Postner, S. M. Block, and E. F. Wieschaus, "Developmental regulation of vesicle transport in drosophila embryos: Forces and kinetics," *Cell*, vol. 92, no. 4, pp. 547–557, 1998.

[6] G. A. Morfini *et al.*, "Pathogenic huntingtin inhibits fast axonal transport by activating jnk3 and phosphorylating kinesin," *Nature Neurosci.*, vol. 12, no. 7, pp. 864–871, 2009.

[7] S. Bhaban, S. Talukdar, and M. Salapaka, "Noise induced transport at microscale enabled by optical fields," in *Proc. Amer. Control Conf.*, 2016, pp. 5823–5829.

[8] K. Svoboda and S. M. Block, "Force and velocity measured for single kinesin molecules," *Cell*, vol. 77, no. 5, pp. 773–784, 1994.

[9] M. J. Schnitzer and S. M. Block, "Kinesin hydrolyses one ATP per 8-nm step," *Nature*, vol. 388, no. 6640, pp. 386–390, 1997.

[10] J. A. Spudich, S. E. Rice, R. S. Rock, T. J. Purcell, and H. M. Warrick, "Optical traps to study properties of molecular motors," *Cold Spring Harbor Protocols*, vol. 2011, no. 11, pp. 1305–1318, 2011.

[11] A. Ashkin, J. Dziedzic, J. Bjorkholm, and S. Chu, "Observation of a single-beam gradient force optical trap for dielectric particles," *Opt. Lett.*, vol. 11, no. 5, pp. 288–290, 1986.

[12] T. Aggarwal, "*Novel tools for biophysics research*," Ph.D. dissertation, Dept. Elect. Eng., Univ. Minnesota, Minneapolis, MN, USA, 2012.

[13] T. Aggarwal and M. Salapaka, "Real-time nonlinear correction of back-focal-plane detection in optical tweezers," *Rev. Sci. Instrum.*, vol. 81, no. 12, 2010, Art. no. 123105.

[14] D. K. Jamison, J. W. Driver, and M. R. Diehl, "Cooperative responses of multiple kinesins to variable and constant loads," *J. Biol. Chemistry*, vol. 287, no. 5, pp. 3357–3365, 2012.

[15] M. D. Wang, H. Yin, R. Landick, J. Gelles, and S. M. Block, "Stretching DNA with optical tweezers," *Biophys. J.*, vol. 72, no. 3, pp. 1335–1346, 1997.

[16] Y. Cui and C. Bustamante, "Pulling a single chromatin fiber reveals the forces that maintain its higher-order structure," *Proc. Nat. Acad. Sci.*, vol. 97, no. 1, pp. 127–132, 2000.

[17] S. Roychowdhury, "Breaking perceived limits of performance for nanoscale interrogation & transport systems," Ph.D. dissertation, Univ. Minnesota, Minneapolis, MN, USA, 2015.

[18] E. Meyhöfer and J. Howard, "The force generated by a single kinesin molecule against an elastic load," *Proc. Nat. Acad. Sci.*, vol. 92, no. 2, pp. 574–578, 1995.

[19] A. Kunwar, M. Vershinin, J. Xu, and S. P. Gross, "Stepping, strain gating, and an unexpected force-velocity curve for multiple-motor-based transport," *Current Biol.*, vol. 18, no. 16, pp. 1173–1183, 2008.
[20] D. Materassi, S. Roychowdhury, T. Hays, and M. Salapaka, "An exact approach for studying cargo transport by an ensemble of molecular motors," *BMC Biophys.*, vol. 6, no. 1, 2013, Art no. 14.
[21] S. Bhaban, D. Materassi, M. Li, T. Hays, and M. Salapaka, "Interrogating emergent transport properties for molecular motor ensembles: A semi-analytical approach," *PLoS Comput. Biol.*, vol. 12, no. 11, 2016, Art no. e1005152.
[22] S. Talukdar, S. Bhaban, D. Materassi, and M. Salapaka, "Steady state dynamics of molecular motors reveals load dependent cooperativity," in *Proc. IEEE 55th Conf. Decis. Control*, 2016, pp. 3356–3362.
[23] S. Shastry and W. O. Hancock, "Neck linker length determines the degree of processivity in kinesin-1 and kinesin-2 motors," *Current Biol.*, vol. 20, no. 10, pp. 939–943, 2010.
[24] K. Visscher and S. M. Block, "[38] versatile optical traps with feedback control," *Methods Enzymol.*, vol. 298, pp. 460–489, 1998.
[25] M. J. Lang, C. L. Asbury, J. W. Shaevitz, and S. M. Block, "An automated two-dimensional optical force clamp for single molecule studies," *Biophys. J.*, vol. 83, no. 1, pp. 491–501, 2002.
[26] S. M. Block, "Kinesin motor mechanics: Binding, stepping, tracking, gating, and limping," *Biophys. J.*, vol. 92, no. 9, pp. 2986–2995, 2007.
[27] T. Aggarwal, D. Materassi, R. Davison, T. Hays, and M. Salapaka, "Detection of steps in single molecule data," *Cellular Molecular Bioeng.*, vol. 5, no. 1, pp. 14–31, 2012.
[28] C. Scherer, P. Gahinet, and M. Chilali, "Multiobjective output-feedback control via LMI optimization," *IEEE Trans. Autom. Control*, vol. 42, no. 7, pp. 896–911, Jul. 1997.
[29] R. D. Vale, F. Malik, and D. Brown, "Directional instability of microtubule transport in the presence of kinesin and dynein, two opposite polarity motor proteins," *J. Cell Biol.*, vol. 119, no. 6, pp. 1589–1596, 1992.
[30] J. Gagliano, M. Walb, B. Blaker, J. C. Macosko, and G. Holzwarth, "Kinesin velocity increases with the number of motors pulling against viscoelastic drag," *Eur. Biophys. J.*, vol. 39, no. 5, pp. 801–813, 2010.
[31] S. Roychowdhury, S. Bhaban, S. Salapaka, and M. Salapaka, "Design of a constant force clamp and estimation of molecular motor motion using modern control approach," in *Proc. IEEE Amer. Control Conf.*, 2013, pp. 1525–1530.
[32] S. Roychowdhury, T. Aggarwal, S. Salapaka, and M. V. Salapaka, "High bandwidth optical force clamp for investigation of molecular motor motion," *Appl. Phys. Lett.*, vol. 103, no. 15, 2013, Art no. 153703.
[33] M. Grant and S. Boyd, "CVX: Matlab software for disciplined convex programming, version 2.1." [Online]. Available: http://cvxr.com/cvx. Accessed on: Mar. 2014.
[34] J. J. Gorman, A. Balijepalli, and T. W. LeBrun, "Feedback control of optically trapped particles," in *Feedback Control of MEMS to Atoms*. New York, NY, USA: Springer-Verlag, 2012, pp. 141–177.
[35] K. Visscher, M. J. Schnitzer, and S. M. Block, "Single kinesin molecules studied with a molecular force clamp," *Nature*, vol. 400, no. 6740, pp. 184–189, 1999.
[36] A. Sebastian, D. R. Sahoo, and M. V. Salapaka, "An observer based sample detection scheme for atomic force microscopy," in *Proc. IEEE 42nd Conf. Decis. Control*, vol. 3, 2003, pp. 2132–2137.
[37] D. R. Sahoo, T. De Murti, and V. Salapaka, "Observer based imaging methods for atomic force microscopy," in *Proc. IEEE 44th Eur. Control Conf. Decis. Control*, 2005, pp. 1185–1190.
[38] M. V. Salapaka, M. Dahleh, and P. G. Voulgaris, "Mimo optimal control design: The interplay between the/spl Hscr//sub 2/and the l/sub 1/norms," *IEEE Trans. Autom. Control*, vol. 43, no. 10, pp. 1374–1388, Oct. 1998.
[39] X. Qi, M. Khammash, and M. Salapaka, "A MATLAB package for multiobjective control synthesis," in *Proc. IEEE 40th Conf. Decis. Control*, vol. 4, 2001, pp. 3991–3996.

Shreyas Bhaban (S'15) received the B.Tech degree in instrumentation and control engineering from College of Engineering, University of Pune, Maharashtra, India, in 2011, and the Masters degree in electrical engineering from University of Minnesota, Minneapolis, MN, USA, in 2014. He is currently working toward the Ph.D. degree with the Department of Electrical Engineering, University of Minnesota.

His research interests include systems and controls engineering, nanodynamics and its applications to opto-mechanical systems, and biophysics.

Saurav Talukdar (S'15) received the B.Tech and M. Tech degrees in mechanical engineering from the Indian Institute of Technology, Bombay, Maharashtra, India, and is currently working toward the Ph.D. degree in mechanical engineering at the University of Minnesota, Minneapolis, MN, USA.

His research interests include learning topology of dynamic systems, multiagent systems, and statistical physics.

Mingang Li received the B.S. degree in microbiology from Wuhan University, Wuhan, Hubei, China, in 1982, the M.S. degree in microbiology from the Chinese Academy of Science, Beijing, China, in 1984, and the Ph.D. degree in genetics from Cologne University, Köln, Germany, in 1989.

He is currently a Research 6 staff member in Dr. Tom Hays's lab with the Department of Genetics, Cell Biology and Development, University of Minnesota, Minneapolis, MN, USA. His research interests include structures and functions of molecular motors, neuronal transport, and neurodegeneration.

Thomas Hays received the B.S. degree in zoology in 1976 and the Ph.D. degree in biology in 1985 from the University of North Carolina, Chapel Hill, NC, USA. He received the postdoctoral degree in 1985–1989 with the Department of Molecular, Cellular, and Developmental Biology, University of Colorado, Boulder in the laboratory of Margaret T. Fuller.

He subsequently joined the Faculty with the Department of Genetics and Cell Biology, University of Minnesota, Minneapolis, MN, USA, in 1989. He is currently a full-time professor with the Department of Genetics, Cell Biology, Genetics and Development, University of Minnesota. The Hays Laboratory is applying genetic, molecular, and biochemical approaches in Drosophila to study the molecular regulation of motor proteins and intercellular transport.

Dr. Hays was a recipient of the PEW Foundation Biomedical Scholar Award (1991) and the American Heart Established Investigator Award (1999).

Peter Seiler (M'10) received the Ph.D. in mechanical engineering from the University of California, Berkeley, CA, USA in 2001. His graduate research focused on coordinated control of unmanned aerial vehicles and control over wireless networks.

From 2004 to 2008, he worked at the Honeywell Research Labs on various aerospace and automotive applications, including the redundancy management system for the Boeing 787, sensor fusion algorithms for automotive active safety systems, and re-entry flight control laws for NASA's Orion vehicle. Since joining the University of Minnesota in 2008, he has been working on fault-detection methods for safety-critical systems and advanced control techniques for wind turbines and unmanned aircraft.

Murti Salapaka (SM'13) received the B.Tech. degree in mechanical engineering from the Indian Institute of Technology Madras, Chennai, Tamil Nadu, India, in 1991 and the M.S. and Ph.D. degrees in mechanical engineering from the University of California, Santa Barbara, CA, USA, in 1993 and 1997, respectively.

From 1997 to 2007, he was a Faculty Member with the Electrical and Computer Engineering Department, Iowa State University, Ames, IA, USA. He is currently a Faculty Member with the Electrical and Computer Engineering Department, University of Minnesota, Minneapolis, MN, USA. His research interests include nanotechnology, multiple-objective robust control, and distributed and structural control.